tvst

https://doi.org/10.1167/tvst.8.3.32

Article

Tracking the Reflective Light Particles Spreading on the Cornea: An Emerging Assessment for Tear Film Homeostasis

Hung-Yin Lai[1,*], Ming-Tse Kuo[1,*], Po-Chiung Fang[1], Chi-Chang Lin[2], Chun-Chih Chien[3], Wan-Hua Cho[1], Alexander Chen[1], and Ing-Chou Lai[1]

[1] Department of Ophthalmology, Kaohsiung Chang Gung Memorial Hospital and Chang Gung University College of Medicine, Kaohsiung, Taiwan
[2] Department of Chemical and Materials Engineering, Tunghai University, Taichung, Taiwan
[3] Department of Laboratory Medicine, Kaohsiung Chang Gung Memorial Hospital and Chang Gung University College of Medicine, Kaohsiung, Taiwan

Correspondence: Ming-Tse Kuo, Department of Ophthalmology, Kaohsiung Chang Gung Memorial Hospital and Chang Gung University College of Medicine, Kaohsiung, Taiwan, No. 123, Dapi Road, Niaosong District, Kaohsiung City 833, Taiwan (R.O.C.). e-mail: mingtse@cgmh.org.tw

Received: 30 October 2018
Accepted: 15 April 2019
Published: 4 June 2019

Keywords: tear film homeostasis; tear hydrodynamics; dry eyes; contact lens; orthokeratology

Citation: Lai H-Y, Kuo M-T, Fang P-C, Lin C-C, Chien C-C, Cho W-H, Chen A, Lai I-C. Tracking the reflective light particles spreading on the cornea: an emerging assessment for tear film homeostasis. Trans Vis Sci Tech. 2019;8(3):32, https://doi.org/10.1167/tvst.8.3.32

Purpose: To implement an emerging noninvasive approach for assessing the dynamic tear film (TF) homeostasis.

Methods: The video records of dynamic TF from 12 healthy orthokeratology lens wearers were obtained by a clinically available TF analyzer and decomposed as image sequences. The trajectories of TF particles were analyzed by two tracking models, the full-span model (FSM) and the fixed-duration model (FDM). FSM tracked a particle for a complete opening blink cycle, while FDM tracked 1 second of the same cycle. A power-law fitting operation $\mathrm{MMS}(t) = \alpha \times t^{-\beta}$ was used to extract homeostasis markers based on the tracking model for each subject.

Results: Comparing two tracking models ($N = 6$), only one subject had statistical difference in averaged momentary moving speed (MMS; $P = 0.0488$), while none had significant difference in averaged momentary moving direction (MMD). However, both models showed good correlations in average MMS ($\rho = 0.94$, $P = 0.0048$) and MMD ($\rho = 1.00$, $P < 0.0001$) and all extracted homeostasis markers [α, β, MMS(0.1), and MMS(2.0)]. Assessing interblink reliability in these markers under FDM tracking ($N = 12$), only one subject in the MMS (0.1) and another subject in the MMS (2.0) were outside 95% limits of agreement, respectively.

Conclusions: FDM is a good alternative to FSM and has tracking properties of higher efficiency and easier implementation. The homeostasis markers under FDM tracking showed a good interblink consistence; therefore this approach will be a promising method for analyzing dynamic TF homeostasis in future practice.

Translational Relevance: FDM analytical architecture can practice the past experimental platform on a TF analyzer to obtain homeostasis markers of TF.

Introduction

According to the consensus of the Tear Film and Ocular Surface Society in the Dry Eye Workshop II, dry eye is a multifactorial disease of the ocular surface characterized by a lack of tear film (TF) homeostasis.[1] The diagnosis of dry eye disease (DED) should meet the criteria of a symptomatic survey (e.g., Ocular Surface Disease Index) and one of the three homeostasis markers of TF.[2] Among the three markers (noninvasive tear breakup time [NITBUT], TF osmolarity, and ocular surface staining), only NITBUT could assess the dynamic expression of TF homeostasis.[3–5] However, this test assesses the TF dynamics under unnatural circumstances because the subject must forcefully keep his or her eyes open at least 10 seconds, and many subjects, such as children, failed to complete this test. In addition, DED is a multifactorial disease that requires different methods

to clarify TF dynamics. NITBUT primarily reflects the dynamics of the TF in terms of TF stability and less in terms of viscosity. TF viscosity is the property of tears that opposes the relative motion between superficial and deep surfaces of TF that are moving at different velocities, that is, the friction between TF molecules, generally recognized as mucins being the main component, accompanied by other tear proteins and lipids.[6] Moreover, patients who fulfilled the symptom criteria of DED without positive results from three homeostasis markers are now classified as neuropathic pain or preclinical dry eye status. For these patients, the possibility of incomplete TF homeostasis assessment, especially in the TF dynamics, cannot be excluded.[7] Thus, an alternative way for diagnosing DED by focusing on the assessment of dynamic TF homeostasis is needed.

Owens and Phillips[8] previously proposed a novel way for assessing dynamic TF homeostasis by observing the movement of reflective light particles on TF, which might reflect the TF viscosity.[6,9] The reflective TF particles have not been elucidated in terms of their compositions, and these naturally occurring particles were presumed to be reflective dusts[10] or mucin-contaminated lipid particles[8] that are produced at tear refreshing during eyelid closure. Nonetheless, this approach has not been widely applied and was used only in a self-assembled experimental platform.[2] Requiring a solid platform, an experienced eye-care practitioner with a superb photography technique, a self-programming image software package, and a standard analytical model may have prevented their method from becoming a standard assessment tool.[8,10] Until recently, a commercialized TF analyzer (Keratograph 5M; Oculus, Inc., Arlington, WA, USA) provided a simple and standard environment for technicians to easily perform this video examination. Furthermore, some free packages of image software are now available to process this video record for subsequent analysis. Therefore, the method is very promising regarding filling the gap between experimental task and real-world practice and could be an emerging approach for assessing TF dynamics clinically.[2]

Therefore, the primary objective of the study was to implement this approach for assessing dynamic TF homeostasis by using a clinically available TF analyzer to fill the gap between basic research and clinical care. The second objective was to establish a standard analytical model and extract potential TF homeostasis markers based on our dynamic assessment for use in future clinical practice.

Methods

Participants

Dynamic TF videos were obtained from 12 orthokeratology lens wearers who participated in a prospective observation study for investigating the bioburden assessment of contact lens (CL) wear between August 2016 and July 2017 in Kaohsiung Chang Gung Memorial Hospital (CGMH). All procedures involving human participants adhered to the tenets of the Declaration of Helsinki and the ARVO statement on human subjects. Institutional review board/ethics committee approval was obtained from the committee of medical ethics and human experiments of CGMH. These participants were healthy individuals aged 12 to 18 years old who were without systemic diseases. All participants and their legal representatives were clearly informed about the aim and procedure of this study and signed the informed consent. Each subject received a complete ocular examination and dynamic TF examinations by masked examiners. No ocular disease was identified for these subjects.

Examination of Dynamic TF

For each subject, only one eye was randomly selected for dynamic TF assessment. Before the test, each subject was instructed to blink naturally during the examination. With a TF analyzer (Keratograph 5M), the TF dynamic was observed under two illumination sources of white diodes and the recording video was obtained. At the beginning of the examination, the examiner focused on the anterior corneal surface under 1.4× magnification to make mobile reflective light particles clearly visible on the TF. The recorder was then started to obtain a dynamic TF video. Generally, three to four blink cycles were recorded in a 10-second video record (Supplementary File S1).

Tracking the Trajectories of TF Particles

Each dynamic TF video was decomposed into image frames with a time interval of 0.1 second using a free online program (Free Video JPG Converter, version 5.0.101.201; Digital Wave Ltd., https://www.dvdvideosoft.com/products/dvd/Free-Video-to-JPG-Converter.htm), and three to four sets of sequence

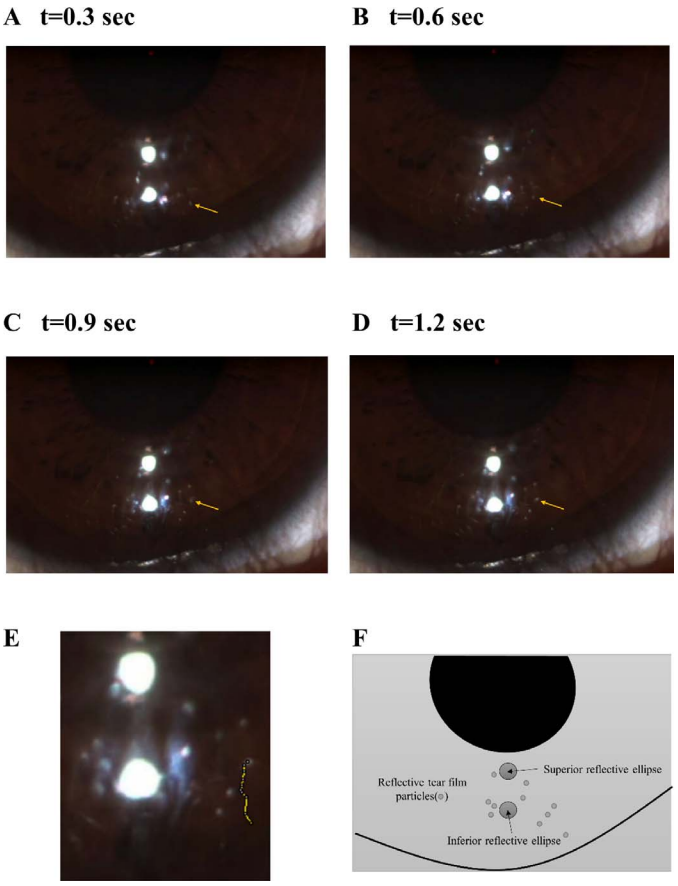

Figure 1. A representative motion of a reflective light particle on the TF. (A–D) The position of the TF particle at 0.3, 0.6, 0.9, and 1.2 seconds, respectively. (E) The 1-second linked pathway of the TF particle with a time interval of 0.1 second shown by a locally amplified image. (F) The anatomical illustration of one decomposed image frame from a video record using a TF analyzer (Keratograph 5M). The superior and inferior reflective ellipses were used as proofs of a stable image and also were used to normalize the positions of TF particles for correcting small deviations from involuntary eye movement at tracking particles among different image frames.

images from opening blink cycles were obtained for each subject (Supplementary File S2). The qualified sequence image set must meet clearly visible TF particles under stable and undistorted superior and inferior reflective ellipses (Fig. 1). Under the grid coordinate for sequence image with 720 × 540 pixels, the pixel-base loci of a target reflective light spot (TF particle) and the mass centers of superior and inferior bright ellipses reflected from light sources (Fig. 1) were then manually tracked and automatically recorded by Manual Tracking, a plugin program of ImageJ (1.42q; https://imagej.nih.gov/ij/plugins/track/track.html; provided in the public domain by Wayne Rasband, National Institute of Health, Bethesda, MD, USA), for the qualified sequence image set of each subject (Supplementary File S3).

Standardization of the Positional Coordinate for Each TF Particle

For an arbitrary frame (n), the pixel coordinates (x_{sn}, y_{sn}) and (x_{in}, y_{in}) of mass centers of superior and inferior ellipses and the intercenter pixel distance [$d_{cn} = \sqrt{(x_{sn} - x_{in})^2 + (y_{sn} - y_{in})^2}$] of the two ellipses were used to normalize the positions of TF particles to minimize the small deviation from natural ocular microfluctuations when tracking the target particle among sequence image frames.[11,12] For a TF particle at pixel coordinate (x_n, y_n), its normalized position (X_n, Y_n) was obtained by subtracting the corresponding superior ellipse coordinate and dividing by the intercenter pixel distance in the same frame and formulated as $\left(\frac{x_n - x_{sn}}{d_{cn}}, \frac{y_n - y_{sn}}{d_{cn}}\right)$. The standardized position [$\boldsymbol{X}_n$, $\boldsymbol{Y}_n$] of a TF particle at any frame (n) was obtained using coordinate translation by subtracting its initial normalized position (X_i, Y_i) in the initial traceable frame (i) from the normalized position (X_n, Y_n) of the same particle in the current frame and multiplying with an image-length correction coefficient S [$= 0.7 \times \left(\frac{d \text{ of a target image}}{d \text{ of a reference image}}\right)$], where 0.7 is an approximate pixel length calculated from true diameter (mm) of the superior ellipse measured from a reference image with a ruler divided by the pixel number of this diameter, that is, [$S \times (X_n - X_i)$, $S \times (Y_n - Y_i)$].

Analytical Models of Dynamic TF Homeostasis Based on TF Tracking Algorithms

Two analytic modalities for objectively extracting the features of trajectories of the TF particles were compared in this study. A presumed gold standard, the full-span modal (FSM), was used to analyze the moving behaviors of three TF particles during a complete opening blink cycle with qualified sequence images (Fig. 2). An alternative model with potentially higher efficiency, the fixed-duration model (FDM), was proposed to analyze the spreading of three to six TF particles for 1 second immediately after stabilization of superior and inferior reflective ellipses in the same blink cycle (Fig. 2). For both models, the selection of the particles in an opening cycle must meet the following criteria. First, at least one TF particle is selected from the initiating frame within 0.4

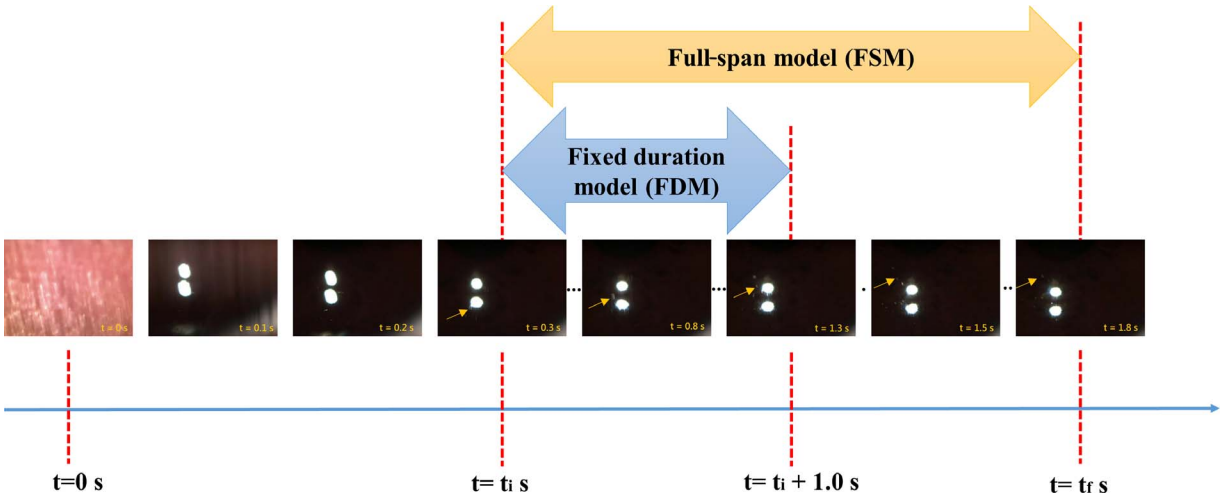

Figure 2. A standardized time-serial image frames decomposed by a dynamic TF video record using a TF analyzer (Keratograph 5M) for full-span and fixed-duration models (FDM). The stable and traceable image was defined by visible reflective TF particles with nondistorted superior and inferior reflective ellipses. In this case, the image frame at 0.3 seconds (t_i) was defined as the qualified image for initiating tracking for both models, while image frames at 0.1 and 0.2 seconds were unqualified due to their oblique and vertically elongated reflective ellipses. As compared to passively terminating image tracking at the end of the image series due to eyelid closure or disappearance of all traceable TF particles in the FSM, the final image frame was predetermined by t_i at 1.3 ($t_i + 1.0$) seconds in the FDM.

seconds ($t_i \leq 0.4$ in Fig. 2). Second, each TF particle must be clearly visible over 10 image frames (0.1-second interval and total duration over 1 second). Third, the TF particles crossing over the superior and inferior ellipses are excluded.

Extracting the Dynamic Homeostasis Markers of the TF Particle

The momentary moving speed (MMS) and direction of a TF particle p at moment $t_{\underline{[(n)+(n+1)]}}$ were defined as the positional change from frame n^2 to frame $n+1$ with a time interval of 0.1 second and were calculated with $\left[\frac{\sqrt{(X_{n+1}-X_n)^2+(Y_{n+1}-Y_n)^2}}{0.1}\right]_p$ and $\left\{\left[\tan^{-1}\frac{(X_{n+1}-X_n)}{(Y_{n+1}-Y_n)}\right]_p \times \frac{180}{\pi}\right\}$, respectively. The speed was designated as a positive displacement per second if a TF particle moved superiorly and vice versa, while the direction was designated as a positive angle if a TF particle moved nasally and vice versa. The averaged momentary speed and direction of different particles presented at the same moment were abbreviated as MMS (averaged momentary moving speed) and MMD (averaged momentary moving direction). For each subject, the mean, median, maximum, minimum, and first and third quartiles of the MMS and MMD from different moments were recognized as features of the tear-spreading profile and obtained according to the two analytical models, FSM and FDM, respectively. Because the initial frame and duration presenting stably detectable TF particles may be different among subjects, and even among different blink cycles of the same subject, the power-law fitting for available MMS data was therefore used to extract two estimators, the initial MMS [MMS($t = 0.1$ second)] and the final MMS [MMS($t = 2.0$ second)], by $\mathrm{MMS}(t) = \alpha \times (t)^{-\beta}$, where α is the scaling factor, β is the power factor, and t is the time variable defined in Figure 2.

Statistical Analysis

All the extracted features of the TF dynamics were calculated using a spreadsheet program (Excel 2016; Microsoft, Redmond, WA, USA). The Excel add-in program, Solver (Microsoft), was used to perform the power-law fitting and extract the model parameters α and β. Using free online statistical software (Social Science Statistics; https://www.socscistatistics.com/), the Mann-Whitney U test was used to examine the parametric differences of MMS and MMD determined by FSM and FDM. Spearman ρ was used to examine the correlation of the same parameter or estimator in the two models. Moreover, the Bland-Altman difference plot was used to analyze the reliability of each FDM parameter obtained from two different blink cycles within the same TF dynamic test. Statistical significance was recognized at $P < 0.05$.

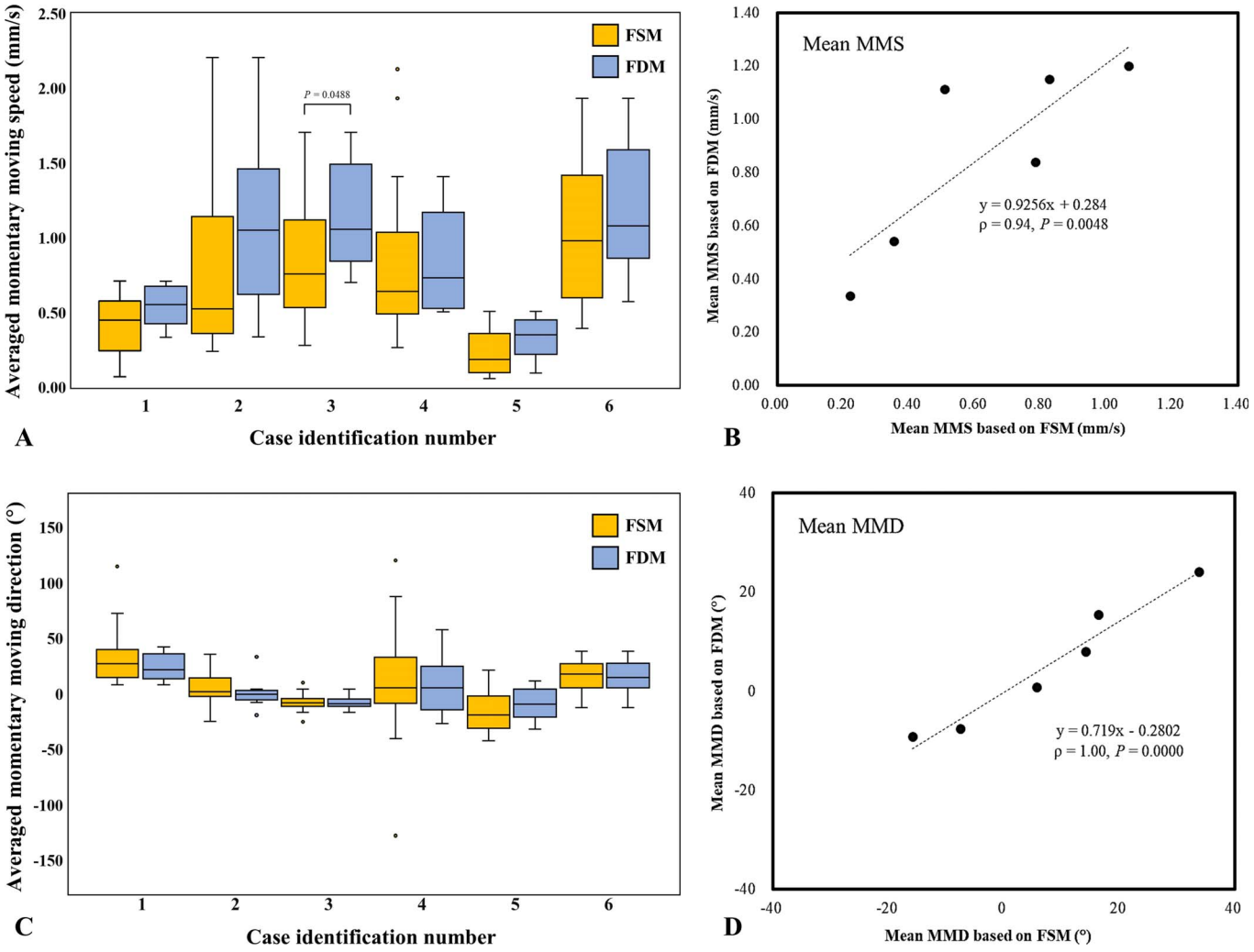

Figure 3. The profiles of averaged momentary moving speeds (MMS) and averaged momentary moving directions (MMD) of TF particles at different moments based on FSMs and FDMs for the first qualified blink cycle of each subject ($n = 6$). (A) Comparing the MMS profile determined by the two analytical models. (B) Correlation of the mean MMS of all moments between FSM and FDM. (C) Comparing the MMD profile determined by FSM and FDM. (D) Correlation of the mean MMD of all moments between FSM and FDM.

Results

The Spreading Speed Profile of the TF Particle

Generally, the TF particle was initially and stably detectable at approximately 0.2 to 0.4 seconds (t_i) after entering an opening phase of a blink cycle (Fig. 2). The visible TF particle was presented as a decelerated motion, and the higher MMSs obtained during the 1-second initial tracking period (t_i to $t_i + 1.0$) for a subject were included in both models, FSM and FDM. Six participants had their own spreading speed profiles based on either FSM or FDM (Fig. 3A). Under the two analytical models, each subject demonstrated different moving speed profiles, and case 3 showed significantly different MMS profiles between FSM and FDM. However, the mean MMS demonstrated a high correlation between the two analytical models for the six subjects (Fig. 3B).

The Moving Direction Profile of the TF Particle

The TF particle generally moves upward with slight nasal or temporal deviation following eyelid opening. It was much easier to include the large deviation angle (cases 1 and 4; Fig. 3C) from a longer assessment period adopted by FSM, probably due to fatigue and unfocused eyeball rotation during examination. However, there was no significant difference

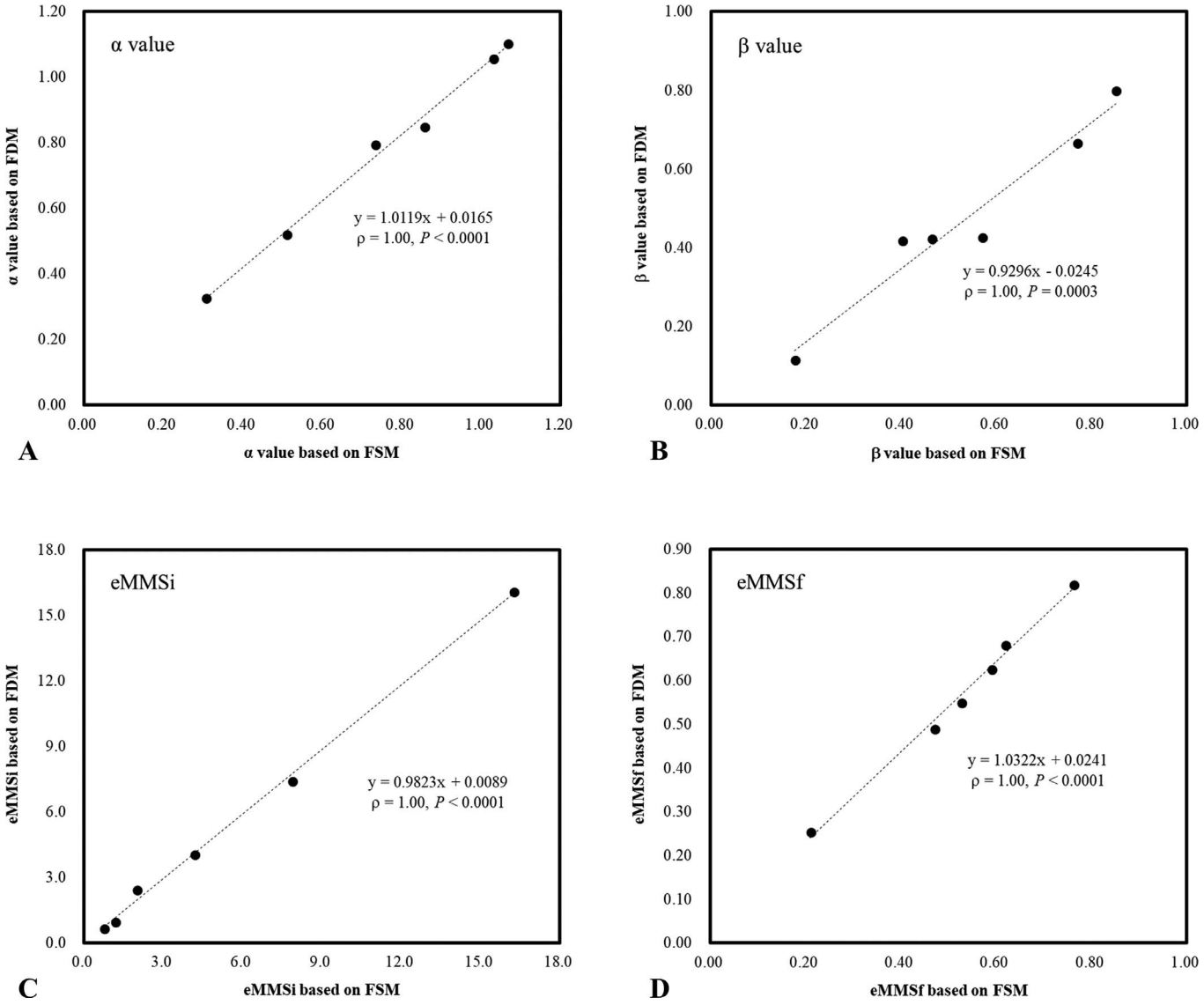

Figure 4. The estimated MMS derived from power-law fitting analysis for dynamic TF particles at different moments based on FSMs and FDMs for the first qualified blink cycle of each subject ($n = 6$). After power-law fitting for the estimated MMS [MMS(t)], $\mathrm{MMS}(t) = \alpha \times (t)^{-\beta}$, parameters α and β were determined using traceable MMS obtained from the two analytical models. The equivalents of initial MMS [eMMSi; MMS (0.1 second)] and final stabilized MMS [eMMSf; MMS (2.0 seconds)] of TF particles for each subject were then obtained. (A–D) Correlation analysis for homeostasis markers α, β, eMMSi, and eMMSf of MMS(*t*) between FSM and FDM, respectively.

on the MMD profile between FSM and FDM for each subject (Fig. 3C). Besides, the mean MMD showed highly positive correlation between FSM and FDM for these subjects (Fig. 3D).

Power-Law Fitting MMS for Estimating the Initial and Final MMS

After power-law fitting analysis for time-serial MMSs, parameters α, β, the equivalent of initial MMS (eMMSi), and final stabilized MMS (eMMSf) of TF particles in the first qualified blink cycle for each subject were obtained based on FSM and FDM, respectively. We found all four of the derived MMS parameters for the six subjects revealed significant correlations between the two analytical models (Fig. 4). For the six subjects analyzed by either FSM or FDM, we observed that eMMSi was determined by both α and β, while eMMSf was determined only by α.

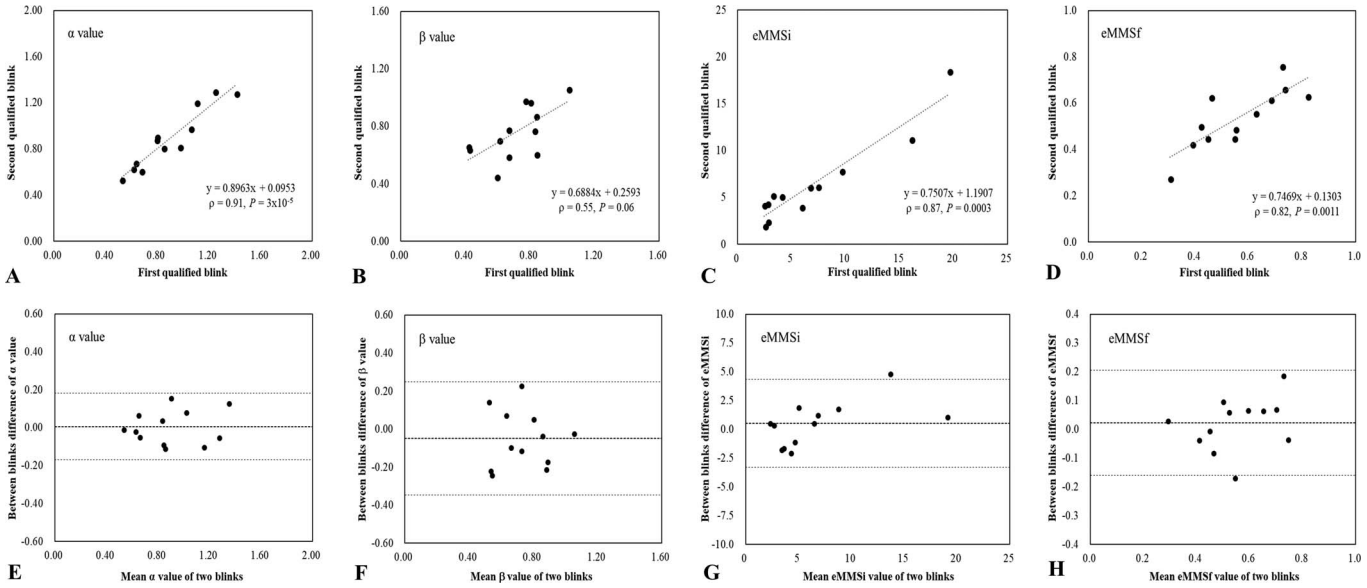

Figure 5. Correlation and agreement on the estimated MMS of TF particles based on the FDM between the first and second qualified blink cycles of each subject ($n = 12$). (A–D) Correlation analysis for homeostasis markers α, β, eMMSi, and eMMSf of the estimated MMS between the two blink cycles, respectively. (E–H) Agreement analysis by the Bland-Altman difference plot for homeostasis markers α, β, eMMSi, and eMMSf between the two blink cycles, respectively. The *upper* and *lower dash lines* represent the 95% limits of agreement.

Interblink Agreement Analysis for the Estimated MMS of TF Particles Based on the FDM

FDM was selected for agreement analysis of the estimated MMS of TF particles between blinks because it was equivalently efficient in FSM after power-law fitting transformation (Fig. 4). The first and second qualified blink cycles for a total of 12 orthokeratology subjects were analyzed. The power-law fitting parameter α was highly correlated between the two blink cycles, while parameter β had only marginally significant correlation (Fig. 5A,B). However, both eMMSi and eMMSf showed significant correlations between two blinks (Fig. 5C,D). From the Bland-Altman plot analysis for the two blink cycles (Fig. 5E–H), the MMS parameters α and β for all subjects were within 95% limits of agreement; only one subject (case 6) was slightly beyond the upper limit of eMMSi, and another subject (case 7) was slightly beyond the lower limit of eMMSf. Consequently, the estimated MMSs derived from power-law fitting for two blink cycles in a TF dynamic examination demonstrated very good agreements.

Discussion

At present, breakdown of TF homeostasis is regarded as the core characteristic of DED. Multidimensional assessment of TF homeostasis is therefore necessary in diagnosing multifactorial DED. To assess dynamic TF homeostasis in a more natural way, we observed the behavior of TF particles and then implemented a standardized approach by tracking TF particles in the video examination acquired from a commercialized TF analyzer. We further compared two analytical models, FSM and FDM, to trace the TF particle to determine the moving speed and direction of TF spreading. We found FDM to be an efficient alternative for FSM, and the speed features extracted by means of power-law fitting were highly correlated between the two models. Moreover, we demonstrated these speed features, potential dynamic TF homeostasis markers, had good agreement between two opening blink cycles for the same subject.

Owens and Phillips[8] used a self-assembled platform to assess the TF dynamics and proposed two descriptors of tear spreading: initial velocity and time to stabilization. They found the particle velocity decay with time, and $\mathrm{MMS}(t) = -2.21 \times \mathrm{Ln}(t) + 0.02$ 5 was the least-squares fitted line regressed from 20 normal subjects. For each case, the time zero was defined as that frame in which the cornea was first fully visible after a blink (equivalent to the frame at 0.1 second in our study shown in Fig. 2), and the initial velocity was obtained by extrapolating the velocity-to-time curve at 0.04 seconds. Moreover,

time to stabilization was obtained by extrapolating the best-fitting logarithmic function to determine the intercept with the abscissa. Owens and Phillips[8] concluded that the mean initial velocity and time to stabilization for normal subjects was 7.34 ± 2.73 mm/s and 1.05 ± 0.30 s, respectively. For future popular applications based on a clinically available TF analyzer, we standardized the TF particle-tracking procedure, minimized the effect of involuntary eye movement,[11,12] and compared the particle-tracking model for efficiently obtaining the dynamic homeostasis markers (Fig. 2). Furthermore, we adopted the power-fitting function $\mathrm{MMS}(t) = \alpha \times t^{-\beta}$ for each subject to characterize individual TF spread and proposed the estimated initial and final velocities, respectively, at 0.1 and 2.0 seconds (Figs. 4 and 5) to replace the initial velocity and time to stabilization proposed by Owens and Phillips[8] for avoiding the unintuitive extrapolating operation. Varikooty et al.[10] also used a self-assembled system to track the TF particles over CLs to estimate TF spread and stability. Tracking the TF particle over CLs is also implementable by the TF analyzer used in this study (data not shown).

CL wear is an important risk factor of DED, but it is a modifiable risk factor under prudent monitoring and management for wearers with unstable TF.[13,14] Pediatric CL wearers with unstable TF often have fewer complaints for their dry eye symptoms, which may lower their guardians' awareness of their underlying DED.[15] TF homeostasis breakdown in pediatric orthokeratology lens wearers, at least temporarily, has been noticed.[16–19] Children may have more difficulty completing tests, for example, due to their reluctance to keep their eyes open in a NIKBUT test or fear of mini-invasive tear collection for a tear osmolarity test. Consequently, pediatric orthokeratology lens wearers were selected as our targets for dynamic TF assessment using this emerging technique.

For exploring the dynamic TF steady state, video recording with corresponding analysis is the basic element, and no single test can guarantee 100% response of the homeostasis. Comparing these capable noninvasive methods, NITBUT importantly assesses the TF stability aspect by detecting the breakup point of TF under forceful eyelid-opening status, which is an index of maximal tolerability to keep TF integrity determined by many factors.[20] To observe the height of tear meniscus with time is another aspect, indicating the amount of the tear fluid reservoir on the ocular surface is balanced under gravity and nasolacrimal drainage during eyelid opening.[21,22] To detect the thickness change and to observe the spreading pattern of the lipid layer of TF during natural blinks are promising homeostasis markers because meibomian gland dysfunction has been well recognized as a major cause of DED.[23,24] To assess the TF particle spread in the diagnosis of DED,[2] a reduction in TF particle velocity was observed in 10 subjects after CL wear, one patient with Sjogren syndrome and one healthy subject after meibomian gland expression.[8,10] These findings supported this technique and have potential applications in assessing dynamic TF homeostasis.

However, the influence from incomplete blinks and the relationship between TF particle movement and lipid tear spread has not been clarified. Moreover, eye-care practitioners are more interested in knowing whether the steady-state markers of this technology reflect the viscosity of TF in order to guide clinical treatment. Therefore, much research is needed in the future to explore these interesting issues.

In conclusion, assessment of dynamic TF homeostasis based on the spread of TF particles is implementable using a clinically available TF analyzer. The proposed tracking model, FDM, is an efficient alternative approach to identifying the homeostasis markers (α, β, eMMSi, and eMMSf) from the TF particle dynamic assessment. These markers in different blink cycles for the same subject showed a highly consistent result. As a result, we believe this assessment will be popularly adopted in the near future as one of the multidimensional approaches for identifying the dynamic TF homeostasis, especially assisted by computer vision technology, for instantly and automatically obtaining the above homeostasis markers.

Acknowledgments

The authors thank Chi-Hsiang Chu, Clinical Trial Center of Kaohsiung Chang Gung Memorial Hospital, for his help in statistical consultation.

Supported by Chang Gung Research Proposal (Grants CMRPG8F0871 and CMRPG8E0341) and the Ministry of Science and Technology (Grant 104-2314-B-182A-101-MY3). The sponsors or funding organizations had no role in the design or conduct of this research.

Disclosure: **H.-Y. Lai**, None; **M.-T. Kuo**, None; **P.-**

C. Fang, None; **C.-C. Lin**, None; **C.-C. Chien**, None; **W.-H. Cho**, None; **A. Chen**, None; **I.-C. Lai**, None

*Hung-Yin Lai and Ming-Tse Kuo are equal contributors in this study.

References

1. Craig JP, Nichols KK, Akpek EK, et al. TFOS DEWS II definition and classification report. *Ocul Surf*. 2017;15:276–283.
2. Wolffsohn JS, Arita R, Chalmers R, et al. TFOS DEWS II diagnostic methodology report. *Ocul Surf*. 2017;15:539–574.
3. Methodologies to diagnose and monitor dry eye disease: report of the Diagnostic Methodology Subcommittee of the International Dry Eye WorkShop (2007). *Ocul Surf*. 2007;5:108–152.
4. Downie LE. Automated fear film surface quality breakup time as a novel clinical marker for tear hyperosmolarity in dry eye disease. *Invest Ophthalmol Vis Sci*. 2015;56:7260–7268.
5. Liu H, Begley CG, Chalmers R, Wilson G, Srinivas SP, Wilkinson JA. Temporal progression and spatial repeatability of tear breakup. *Optom Vis Sci*. 2006;83:723–730.
6. Pult H, Tosatti SG, Spencer ND, Asfour JM, Ebenhoch M, Murphy PJ. Spontaneous blinking from a tribological viewpoint. *Ocul Surf*. 2015;13:236–249.
7. Braun RJ, King-Smith PE, Begley CG, Li L, Gewecke NR. Dynamics and function of the tear film in relation to the blink cycle. *Prog Retin Eye Res*. 2015;45:132–164.
8. Owens H, Phillips J. Spreading of the tears after a blink: velocity and stabilization time in healthy eyes. *Cornea*. 2001;20:484–487.
9. Li L, Braun RJ, Driscoll TA, Henshaw WD, Banks JW, King-Smith PE. Computed tear film and osmolarity dynamics on an eye-shaped domain. *Math Med Biol*. 2016;33:123–157.
10. Varikooty J, Keir N, Simpson T. Estimating tear film spread and stability through tear hydrodynamics. *Optom Vis Sci*. 2012;89:E1119–1124.
11. Buehren T, Lee BJ, Collins MJ, Iskander DR. Ocular microfluctuations and videokeratoscopy. *Cornea*. 2002;21:346–351.
12. Zhu M, Collins MJ, Iskander DR. Dynamics of ocular surface topography. *Eye (Lond)*. 2007;21:624–632.
13. Stapleton F, Alves M, Bunya VY, et al. TFOS DEWS II epidemiology report. *Ocul Surf*. 2017;15:334–365.
14. Colorado LH, Alzahrani Y, Pritchard N, Efron N. Time course of changes in goblet cell density in symptomatic and asymptomatic contact lens wearers. *Invest Ophthalmol Vis Sci*. 2016;57:2888–2894.
15. Greiner KL, Walline JJ. Dry eye in pediatric contact lens wearers. *Eye Contact Lens*. 2010;36:352–355.
16. Tao A, Cai C, Shen M, et al. Tear menisci after overnight contact lens wear. *Optom Vis Sci*. 2011;88:1433–1438.
17. Na KS, Yoo YS, Hwang HS, Mok JW, Kim HS, Joo CK. The influence of overnight orthokeratology on ocular surface and meibomian glands in children and adolescents. *Eye Contact Lens*. 2016;42:68–73.
18. Nieto-Bona A, Nombela-Palomo M, Felipe-Marquez G, Teus MA. Tear film osmolarity in response to long-term orthokeratology treatment. *Eye Contact Lens*. 2018;44:85–90.
19. Li J, Dong P, Liu H. Effect of overnight wear orthokeratology lenses on corneal shape and tears. *Eye Contact Lens*. 2018;44:304–307.
20. King-Smith PE, Begley CG, Braun RJ. Mechanisms, imaging and structure of tear film breakup. *Ocul Surf*. 2018;16:4–30.
21. Johnson ME, Murphy PJ. Temporal changes in the tear menisci following a blink. *Exp Eye Res*. 2006;83:517–525.
22. Uchida A, Uchino M, Goto E, et al. Noninvasive interference tear meniscometry in dry eye patients with Sjogren syndrome. *Am J Ophthalmol*. 2007;144:232–237.
23. Ji YW, Lee J, Lee H, Seo KY, Kim EK, Kim TI. Automated measurement of tear film dynamics and lipid layer thickness for assessment of non-Sjögren dry eye syndrome with meibomian gland dysfunction. *Cornea*. 2017;36:176–182.
24. Yokoi N, Yamada H, Mizukusa Y, et al. Rheology of tear film lipid layer spread in normal and aqueous tear-deficient dry eyes. *Invest Ophthalmol Vis Sci*. 2008;49:5319–5324.